Systematic Theoretical Study on Structural, Stability, Electronic, and Spectral Properties of $Si_2Mg_n^Q$ ($Q = 0$, ±1; $n = 1$–11) Clusters of Silicon-Magnesium Sensor Material

Ben-Chao Zhu[1,2], Ping-Ji Deng[1,2] and Lu Zeng[3]*

[1] School of Public Health and Management, Hubei University of Medicine, Shiyan, China, [2] Center for Environment and Health in Water Source Area of South-to-North Water Diversion, Hubei University of Medicine, Shiyan, China, [3] College of Materials Science and Engineering, Chongqing University, Chongqing, China

By using CALYPSO searching method and Density Functional Theory (DFT) method at the B3LYP/6-311G (d) level of cluster method, a systematic study of the structures, stabilities, electronic and spectral properties of $Si_2Mg_n^Q$ ($n = 1$–11; $Q = 0$, ±1) clusters of silicon-magnesium sensor material, is performed. According to the calculations, it was found that when $n > 4$, most stable isomers in $Si_2Mg_n^Q$ ($n = 1$–11; $Q = 0$, ±1) clusters of silicon-magnesium sensor material are three-dimensional structures. Interestingly, although large size $Si_2Mg_n^Q$ clusters show cage-like structures, silicon atoms are not in the center of the cage, but tend to the edge. The $Si_2Mg_{1,5,6,8}^{-1}$ and $Si_2Mg_{13,4,7,9,10}^{+1}$ clusters obviously differ to their corresponding neutral structures, which are in good agreement with the calculated values of VIP, AIP, VEA, and AEA. |VIP-VEA| values reveal that the hardness of Si_2Mg_n clusters decreases with the increase of magnesium atoms. The relative stabilities of neutral and charged $Si_2Mg_n^Q$ ($n = 1$–11; $Q = 0$, ±1) clusters of silicon-magnesium sensor material is analyzed by calculating the average binding energy, fragmentation energy, second-order energy difference and HOMO-LUMO gaps. The results reveal that the $Si_2Mg_3^0$, $Si_2Mg_3^{-1}$, and $Si_2Mg_3^{+1}$ clusters have stronger stabilities than others. NCP and NEC analysis results show that the charges in $Si_2Mg_n^Q$ ($n = 1$–11; $Q = 0$, ±1) clusters of silicon-magnesium sensor material transfer from Mg atoms to Si atoms except for $Si_2Mg_1^{+1}$, and strong sp hybridizations are presented in Si atoms of $Si_2Mg_n^Q$ clusters. Finally, the infrared (IR) and Raman spectra of all ground state of $Si_2Mg_n^Q$ ($n = 1$–11; $Q = 0$, ±1) clusters of silicon magnesium sensor material are also discussed.

Keywords: silicon-magnesium sensor material, $Si_2Mg_n^{0,\pm1}$ clusters, geometrical structures, electronic properties, spectral properties

INTRODUCTION

Silicon and magnesium are abundant elements on the earth and are widely used in sensor industry. In particular, silicon, as the main material of semiconductor sensors, has always been the research frontier in the field of sensors. As the only stable compound in Mg-Si binary system, Mg_2Si, which has the characteristics of high melting point, high hardness, high modulus of

elasticity and environmentally friendly, is an *n*-type semiconductor material with a band gap of 0.68–1.03 eV (Atanassov and Baleva, 2007). There are many experimental and theoretical studies on silicon-magnesium sensor materials. For example, theoretically, Morris et al. (1958) first used graphite crucible to melt stoichiometric components to prepare high purity single crystal Mg_2Si materials, they found the band gap of Mg_2Si is 0.78 eV. Aymerich and Mula (2010) and Imai et al. (2003) studied the band structure of Mg_2Si using empirical and first-principles pseudopotentials, respectively. Chen et al. (2010) studied the band structure of Mg_2Si and doped Ag, Al elements by using the first-principles pseudopotential plane wave method based on density functional theory (DFT). By using DFT, they obtained the real part, imaginary part and Photoconductivity of Mg_2Si dielectric function as a function of photon energy. Experimentally, the main work on Mg_2Si is focused on the preparation of thin film materials. Wittmer et al. (1979) was the first to fabricate Mg_2Si semiconductor thin films on Si (111) substrates by evaporating Mg atoms films with different thicknesses using an electron gun at a speed of about 40Å/s in vacuum. Boher et al. (1992) used radio frequency magnetron sputtering technology to sputter Mg_2Si targets onto glass materials and Si (111) substrates, and obtained amorphous Mg_2Si films. Song et al. (2003) used pulsed laser deposition (PLD) method to grow Mg_2Si crystal semiconductor thin films nearly 380 nanometers thick on stainless steel substrates at 500° annealing temperature.

All the above theoretical and experimental studies have greatly enriched the research results on the properties of silicon-magnesium sensor material. However, these studies have not touched the fundamental problem, how do the physical and chemical properties of silicon-magnesium compounds change from small systems (several or dozens of atoms) to large systems? Fortunately, small clusters provide a new way to study this system, which can provide insight into the strength and properties of metal bonds (Ju et al., 2015; Sun et al., 2017, 2018; Bole et al., 2018). Cluster material scale is a concept of nanomaterials. It is a relatively stable micro or sub-micro aggregate composed of several or even thousands of atoms, molecules or ions. Its physical and chemical properties usually vary with the number of atoms contained. Cluster studies have successfully helped us to in-depth understand the structure, stability, electronic states and spectral properties of many materials (Jin et al., 2015a,b; Xia et al., 2015; Xing et al., 2016a,b). There are many reports about sensor material study by using cluster method. For example, Yang et al. (2006) used full-muffin-tin-orbital molecular-dynamics (FP-LMTO-MD) method to study the electronic and geometric structures of Ga_nAs_n (*n* = 4, 5, 6) cluster ions. They found that some of the lowest energy structures for the cluster ions are different from those of the corresponding neutral clusters. Dmytruk et al. (2009) produced zinc oxide clusters by laser ablation of bulk powder zinc peroxide in vacuum and studied them by time-of-flight mass spectrometry. By comparing the experimental results with the theoretical calculations of clusters, the most stable structure of $(ZnO)n$ clusters was verified at *n* = 34, 60, and 78.

However, most of the studies on sensor material clusters are carried out in a crystal growth mode, such as AsGa and ZnO,

where the number of different atoms increases in harmony. In this paper, doped clusters will be used to study the materials of silicon-magnesium sensors. To be exact, we doped a small amount of silicon into magnesium element, which increased the number of magnesium atoms around two silicon atoms from 1 to 11, and made them neutral charged, negative charged and positive charged, respectively. Then, we will study the structure, stability, electronic and spectral properties of $Si_2Mg_n^Q$ (*n* = 1–11; *Q* = 0, ±1) clusters of silicide-magnesium materials in detail. The paper is organized as follows: Section Computation Methods describes the computational details, the results are presented and completely discussed in section Results and discussions, and the final conclusions are summarized in section Conclusion.

COMPUTATION METHODS

All structural optimization and infrared Raman spectrum analysis are carried out by using DFT at B3LYP/6-311G (d) basis set level in Gauss 09 program package (Frisch et al., 2014). In order to find the lowest energy state structure of $Si_2Mg_n^Q$ (*n* = 1–11; *Q* = 0, ±1) clusters of silicon-magnesium sensor material, it is necessary to prepare enough initial configurations of Si_2Mg_n clusters. We used the particle swarm optimization (CALYPSO) method (Wang et al., 2010, 2012; Lv et al., 2012) to get the initial structures of pure magnesium clusters. Then, replacing any two Mg atoms with Si atom in the initial Mg_n clusters' structures. CALYPSO method has successfully predicted structures for various systems ranging from clusters to crystal structures (Lu et al., 2013, 2017, 2018; Lu and Chen, 2018; Xiao et al., 2019). In the process of geometric optimization in Gauss 09 package, for neutral clusters, the spin multiplicity of electrons takes into account 1, 3, 5 states, while for charged clusters, it is 2, 4, 6 states, and there is no constraint on the symmetry. Finally, if the optimization results include virtual frequencies, the coordinates of the virtual mode are relaxed until the real local minimum is obtained. On the basis of eliminating imaginary frequency, the potential energy of all optimized ground state structures will reach absolute local minimum.

In order to prove the reliability of the selected B3LYP/6-311G (d) basis set level, the calculated bond length, vibrational frequency, vertical ionization potential (VIP) and vertical electron affinity (VEA)of the neutral Mg_2, Si_2, SiMg clusters by using different methods at the same 6-311G (d) basis set are shown in **Table 1**. As showed in **Table 1**, the calculated values $r(Mg_2)$ = 3.93 Å, $\omega(Mg_2)$ = 44.96 cm^{-1}, $r(Si_2)$ = 2.17 Å, $\omega(Si_2)$ = 540.82 cm^{-1}, VIP(Si_2) = 9.13 eV, and VEA(Si_2) = 2.02 eV, these conclusions are quite agree with the existed experimental results (Huber, 1979; de Heer et al., 1987; Kitsopoulos et al., 1991; Ruette et al., 2005).

RESULTS AND DISCUSSIONS
Geometrical Structures of $Si_2Mg_n^Q$(*n* = 1–11; *Q* = 0, ±1) Clusters of Silicon-Magnesium Sensor Material
The geometries of $Si_2Mg_n^Q$ (*n* = 1–11; *Q* = 0, ±1) clusters of silicon-magnesium sensor material are optimized by using

TABLE 1 | Calculated values of bond length r (Å), frequency ω (cm^{-1}), vertical ionization potential VIP (eV) and vertical electron affinity VEA (eV) for the Mg$_2$, Si$_2$, and SiMg clusters by different methods.

Methods	Mg$_2$				Si$_2$				SiMg			
	r	ω	VIP	VEA	r	ω	VIP	VEA	r	ω	VIP	VEA
B3LYP	3.93	44.96	8.16	0.43	2.17	540.82	9.13	2.02	2.57	288.31	6.77	0.61
B3PW91	3.61	85.29	6.20	0.22	2.31	476.71	8.53	2.79	2.54	325.98	5.84	1.70
PBE	2.78	263.51	4.75	1.68	2.18	531.49	8.15	2.08	2.56	311.01	6.91	0.96
BPV86	2.78	259.56	7.71	0.69	2.18	527.65	7.84	2.08	2.55	306.74	7.94	1.32
MP1PW91	3.60	88.05	6.16	0.21	2.30	484.06	8.54	2.79	2.54	327.96	5.80	1.71
Expt	3.89[a]	45[a]	–	–	2.25[b]	511[b]	>8.49[c]	2.176 ± 0.002[d]	–	–	–	–

[a]Ruette et al. (2005).
[b]Huber (1979).
[c]de Heer et al. (1987).
[d]Kitsopoulos et al. (1991).

the computational method in section Computation Methods. Due to the existence of so many initial structures, the relative energies of all the initial isomers with different spin multiplicities are optimized, but only the lowest energies and a few low-lying energy isomers are given in **Figures 1–3**. In addition, in **Figures 1–3**, in order to compare the effect of Si-doped Mg clusters on the original structure of pure Mg clusters, we also list the lowest energy state structure Mg$_{n+2}$ ($n = 1–11$) of pure Mg clusters optimized by the same method, while the lowest energy state and two metastable structures of neutral Si$_2$Mg$_n^0$, anionic Si$_2$Mg$_n^{-1}$, cationic Si$_2$Mg$_n^{+1}$ ($n = 1–11$) clusters are given. Under each isomer structure, there are three information about the energy difference between the metastable structure and the lowest energy state structure, the symmetry, and the electronic spin state. So, the first structure of Si$_2$Mg$_n^Q$ clusters are all labeled as 0.00 eV, indicating that this structure is the lowest energy state. The latter two are two metastable structures, and the energy difference with the lowest energy state is directly expressed as a non-zero value. It is noteworthy that when n is determined, there are three energy differences on the right side of the lowest energy structure of Mg$_{n+2}$, they are $\Delta E_1 = E(Si_2Mg_n^0)–E(Mg_{n+2})$, $\Delta E_2 = E(Si_2Mg_n^{-1})–E(Mg_{n+2})$, and $\Delta E_3 = E(Si_2Mg_n^{+1})–E(Mg_{n+2})$, notably, E means the ground state energy. Since there are too many structures, we first give a brief introduction to each structure, and then analyze and discuss their growth patterns shortly below.

$n = 1$: *Si$_2$Mg$_1$, Si$_2$Mg$_1^{-1}$, Si$_2$Mg$_1^{+1}$, and Mg$_3$*

The lowest energy structure of neutral Si$_2$Mg1 with spin singlet and C$_S$ symmetry is an isosceles triangle, which are the similar as the ground state of cationic Si$_2$Mg$_1^{+1}$ and pure Mg$_3$ clusters. For anionic Si$_2$Mg$_1^{-1}$, the linear chain (C$_S$, ^{6}A') in which the Mg atom is in the middle position is found to be the most stable isomer. For metastable isomers, two triangular structures for Si$_2$Mg$_1^{+1}$, two linear chain structures for Si$_2$Mg$_1^{-1}$, and one triangular, one linear chain structures for neutral Si$_2$Mg1.

$n = 2$: *Si$_2$Mg$_2$, Si$_2$Mg$_2^{-1}$, Si$_2$Mg$_2^{+1}$, and Mg$_4$*

The ground states of Si$_2$Mg2 (D$_{2H}$, ^{1}AG) and Si$_2$Mg$_2^{-1}$ (C$_{2H}$, ^{2}AG) are parallelograms with a little different shapes. Replacing

any two Mg atoms with Si atoms in the tetrahedral structure of Mg$_4$ (T$_D$, ^{1}A$_1$) forms the lowest energy isomer structure of Si$_2$Mg$_2^{+1}$ (C$_{2V}$, ^{2}B$_2$). All metastable isomers are planar structures, such as trapezoids, triangles and parallelograms.

$n = 3$: *Si$_2$Mg$_3$, Si$_2$Mg$_3^{-1}$, Si$_2$Mg$_3^{+1}$, and Mg$_5$*
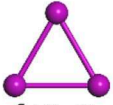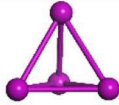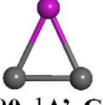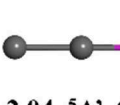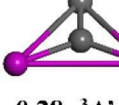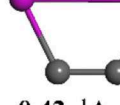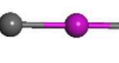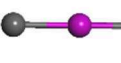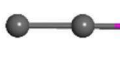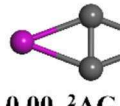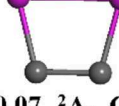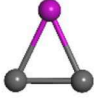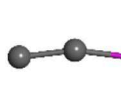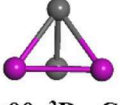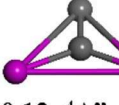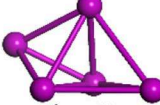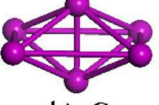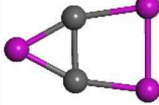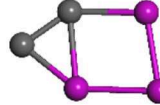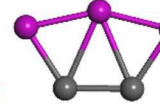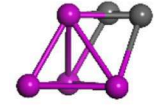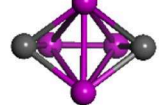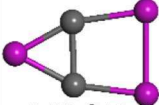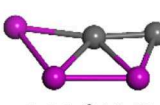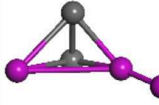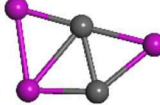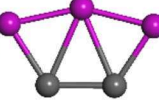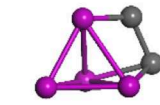
It is impossible to replace two magnesium atoms in the ground state structure of Mg$_5$ (C$_1$, ^{1}A) with silicon atoms to directly form any Si$_2$MgQ 3 ($Q = 0, \pm1$) cluster structure. But the lowest energy isomer structures of Si$_2$Mg3 (C$_S$, ^{1}A') and Si$_2$Mg$_3^{-1}$ (C$_S$, ^{2}A') can be formed by the second metastable isomer structure of Si$_2$Mg2, in where attracting a Mg atom in the same plane outside the trapezoidal silicon-silicon bond. The lowest energy isomer structure of Si$_2$Mg$_3^{+1}$ (C$_1$, ^{2}A) is formed by the ground state of Si$_2$Mg$_2^{+1}$ with a magnesium cap at the top of a magnesium atom. In addition, all metastable isomers exhibit planar structures.

$n = 4$: *Si$_2$Mg$_4$, Si$_2$Mg$_4^{-1}$, Si$_2$Mg$_4^{+1}$, and Mg$_6$*

The lowest energy structure of Mg$_6$ (C$_1$, ^{1}A) is an octahedron. When the two magnesium atoms at the octahedron vertex are replaced by silicon atoms and the lower silicon atoms float up to the plane where the four magnesium atoms are located, the lowest energy state structures of Si$_2$Mg4 (C$_1$, ^{1}A) and Si$_2$Mg$_4^{-1}$ (C$_1$, ^{2}A) are formed. The ground state structure of Si$_2$Mg$_4^{+1}$ (C$_1$, ^{2}A) can be formed by the ground state of Si$_2$Mg$_2^{+1}$attrcating a Mg-Mg bond parallel to the Si-Si bond. All metastable isomers are three-dimensional structures and are directly related to the structure of isomers with small n values.

$n = 5$: *Si$_2$Mg$_5$, Si$_2$Mg$_5^{-1}$, Si$_2$Mg$_5^{+1}$, and Mg$_7$*

The ground state structure of Mg$_7$ (C$_1$, ^{1}A) can be directly formed from Mg$_6$ with a magnesium atom cap on one side of the octahedron. The ground state structures of Si$_2$Mg$_5^{-1}$ (C$_1$, ^{2}A) and Si$_2$Mg$_5^{+1}$ (C$_1$, ^{2}A) are similar, their main body is a triangular prism with a magnesium-silicon-magnesium triangle at the top and bottom, and then a magnesium atom cap at different distances from the side. The lowest energy structure of neutral Si$_2$Mg$_5$ (C$_1$, ^{2}A) is formed when the ground sate structure of Si$_2$Mg$_4$ attracting one magnesium atom. It is easy to see that the first metastable structure of cationic Si$_2$Mg$_5^{+1}$ is the lowest energy state structure of neutral Si$_2$Mg$_5$. Interestingly, the

FIGURE 1 | Optimized geometries of Mg_{n+2} and $Si_2Mg_n^Q$ ($n = 1-4$; $Q = 0, \pm1$) clusters of silicon-magnesium sensor material at B3LYP/6-311+G(d) level. The pink and gray balls present the Mg and Si atoms, respectively.

difference between the first metastable state structure of neutral Si_2Mg_5 and the lowest energy state structure of anionic $Si_2Mg_5^{-1}$ is the orientation of the cap with magnesium atom, the former at the bottom and the latter at the side.

n = 6: Si_2Mg_6, $Si_2Mg_6^{-1}$, $Si_2Mg_6^{+1}$, and Mg_8

The lowest energy structure of Mg_8 (C_1, ^1A) is formed by adding a Mg atom cap to the up down mirror symmetry of Mg_7. When adding a Mg atom cap to the right left mirror symmetry of the lowest energy structure of $Si_2Mg_5^{+1}$, the ground state structures of $Si_2Mg_6^{+1}$ (C_1, ^2A) is formed. The lowest energy structure of neutral Si_2Mg_6 (C_1, ^1A) is as the same as its first metastable structure. The ground state of $Si_2Mg_6^{-1}$(C_1, ^2A) is an

irregular polyhedral cylinder, but its metastable state structures show certain irregularity.

n = 7: Si_2Mg_7, $Si_2Mg_7^{-1}$, $Si_2Mg_7^{+1}$, and Mg_9

The lowest energy state structure of the cationic $Si_2Mg_7^{+1}$ (C_1, ^2A), which is as the same as its second metastable state structure, can be formed by substituting the upper and lower mirror symmetrical Mg atoms for the silicon atoms in the lowest energy state Mg_9 (C_1, ^1A) structure. The ground state of $Si_2Mg_7^{-1}$ (C_1, ^2A) is similar as the first metastable state structure $Si_2Mg_7^{+1}$. The lowest energy structure of the neutral Si_2Mg_7 (C_1, ^2A) has the same main body as the ground state structure of Si_2Mg_4. Interestingly, the second metastable state structure of Si_2Mg_7

FIGURE 2 | Optimized geometries of Mg_{n+2} and $Si_2Mg_n^Q$ ($n = 5$–8; $Q = 0, \pm1$) clusters of silicon-magnesium sensor material at B3LYP/6-311+G(d) level. The pink and gray balls present the Mg and Si atoms, respectively.
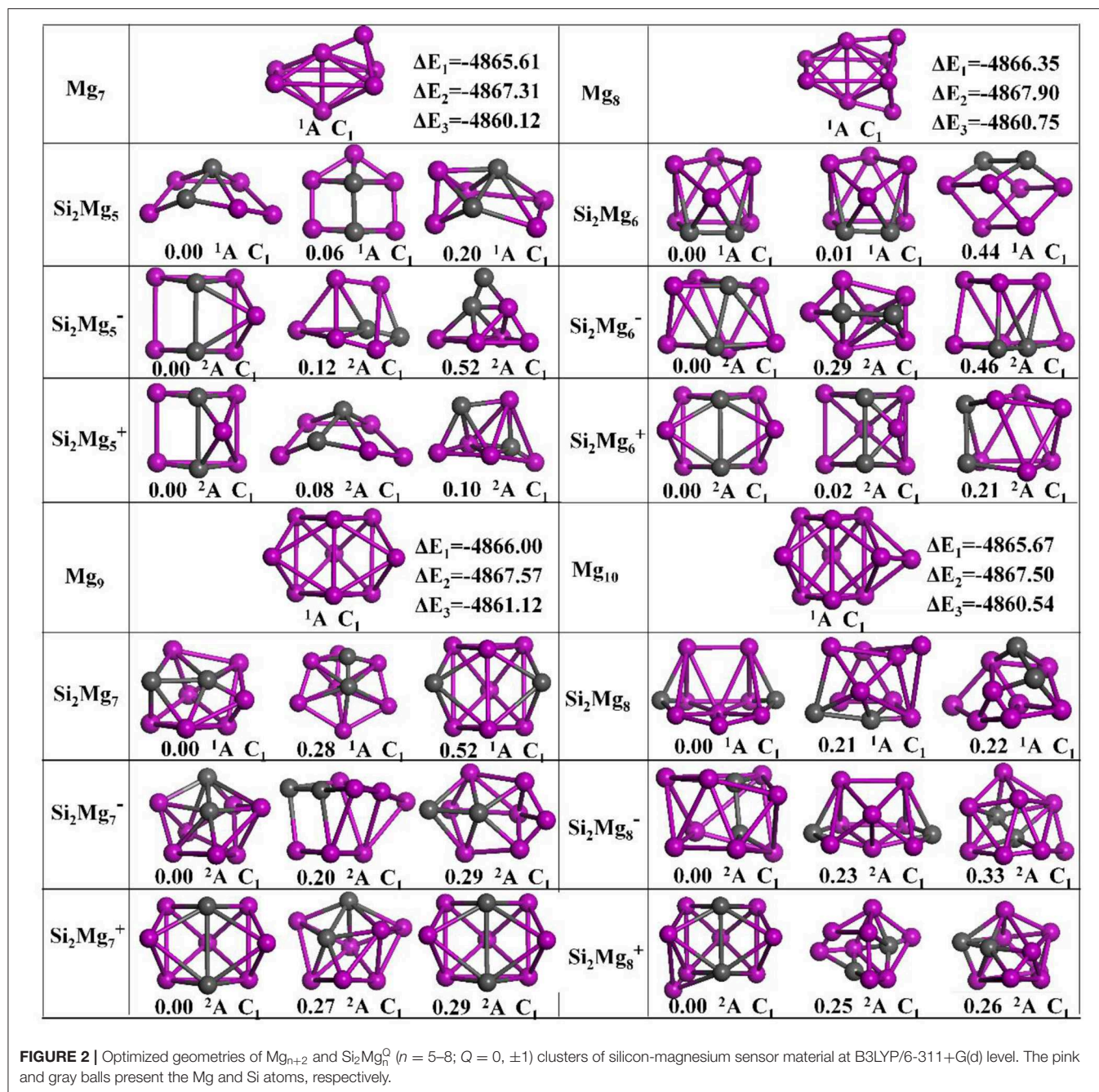
is similar as the ground state structure of $Si_2Mg_7^{+1}$, the only difference is the two silicon atoms are bonded from top to bottom to left.

$n = 8$: Si_2Mg_8, $Si_2Mg_8^{-1}$, $Si_2Mg_8^{+1}$, and Mg_{10}

The lowest energy state structure of the Mg_{10} (C_1, ^1A) is formed by Mg_9 with a magnesium atom on right side. The ground state structure of $Si_2Mg_8^{+1}$ (C_1, ^2A) can be formed by ground state structure of $Si_2Mg_7^{+1}$ with a magnesium cap on left-down side. The lowest energy state structure of neutral Si_2Mg_8 (C_1, ^2A) is similar as the first metastable state structure of $Si_2Mg_8^{-1}$. The

ground state of $Si_2Mg_8^{-1}$(C_1, ^2A) is cage-like structure with one silicon atom trapped on the upper surface. Interestingly, other metastable state structures also present cage-like structures.

$n = 9$: Si_2Mg_9, $Si_2Mg_9^{-1}$, $Si_2Mg_9^{+1}$, and Mg_{11}

When Mg_{10} attracting a magnesium on the left side, it is the lowest energy structure of Mg_{11} (C_1, ^1A). From $n = 9$, it is easy found that no structure of $Si_2Mg_n^Q$ ($Q = 0, \pm1$) can be formed by substituting two magnesium atoms for silicon atoms in Mg_{n+2}. The ground state of $Si_2Mg_9^{-1}$ (C_1, ^2A) is similar as its first metastable state structure. They can be formed based on

FIGURE 3 | Optimized geometries of Mg_{n+2} and $Si_2Mg_n^Q$ (n = 9–11; Q = 0, ±1) clusters of silicon-magnesium sensor material at B3LYP/6-311+G(d) level. The pink and gray balls present the Mg and Si atoms, respectively.
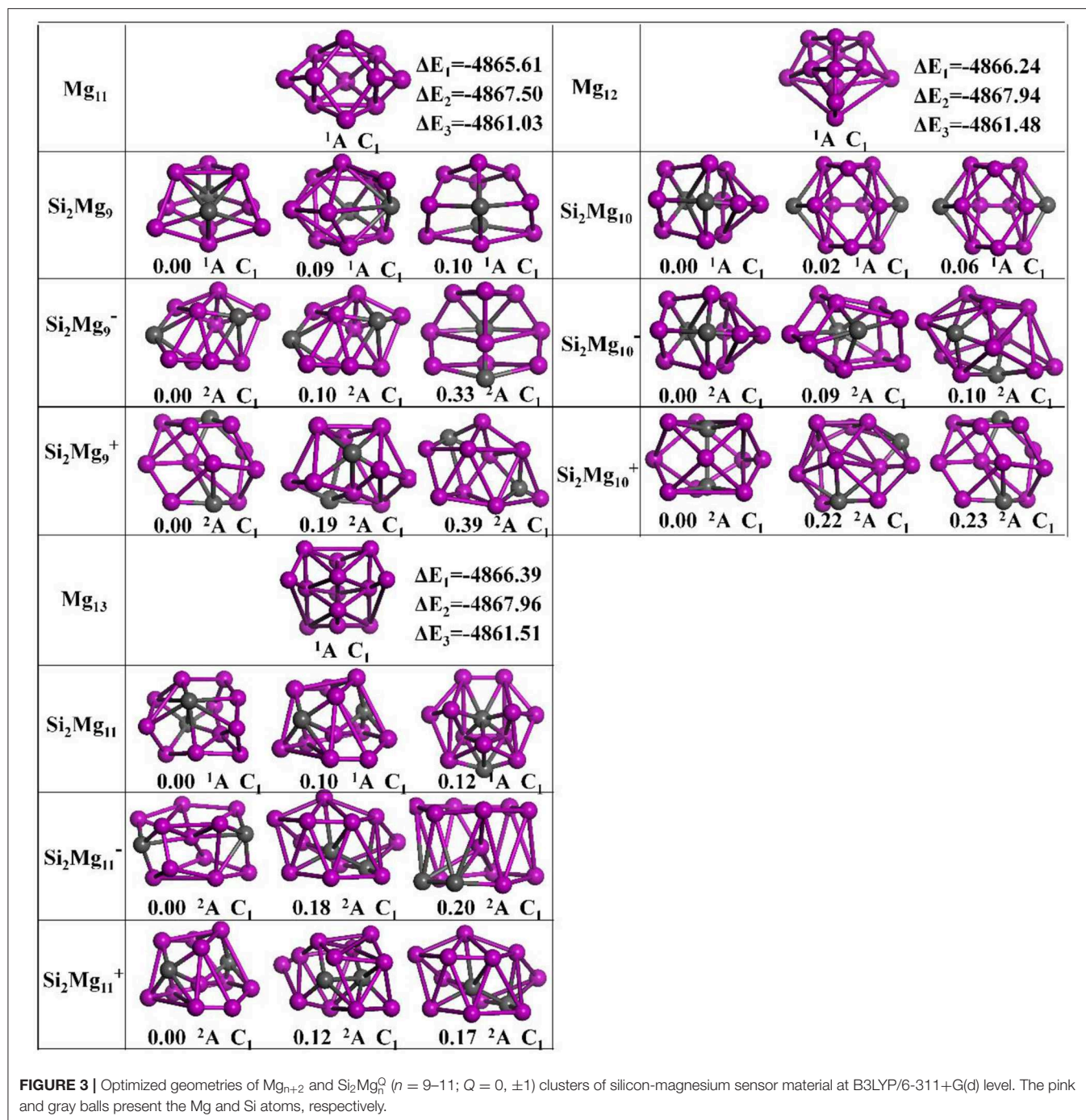
the first metastable structure of $Si_2Mg_8^{+1}$ with a Mg atomic cap. The ground state structure of neutral Si_2Mg_9 (C_1, ^2A) is similar as its second metastable structure and the second metastable structure of $Si_2Mg_9^{-1}$. The lowest energy state structure of $Si_2Mg_9^{+1}$ (C_1, ^2A) is a complex 3D cage-like structure based on the second metastable state of Si_2Mg_4 with attracting more five Mg atoms.

n = 10: Si_2Mg_{10}, $Si_2Mg_1^{-1}0$, $Si_2Mg_1^{+1}0$, and Mg_{12}

The ground state structures of neutral Si_2Mg_{10} (C_1, ^1A) and $Si_2Mg_1^{-1}0$ (C_1, ^2A) are the same and can be formed by the

lowest energy state structure of $Si_2Mg_9^{+1}$ with a magnesium cap. The lowest energy state structure of $Si_2Mg_1^{+1}0$ (C_1, ^2A) is formed by the ground state structure of $Si_2Mg_8^{-1}$ with adding two magnesium atoms. All the metastable structures present 3D structures, and some of them can easily be found to be associated with the cluster structure discussed earlier. For example, the metastable structure of neutral Si_2Mg_{10} can be formed by the ground state of neutral Si_2Mg_8 with adding two Mg atoms.

n = 11: Si_2Mg_{11}, $Si_2Mg_1^{-1}1$, $Si_2Mg_1^{+1}1$, and Mg_{13}

The lowest energy structures of Si_2Mg_{11} (C_1, ^1A), $Si_2Mg_1^{-1}1(C_1, {}^2A)$, $Si_2Mg_1^{+1}1(C_1, {}^2A)$ show cage structures, but no silicon atom located the cage center. By using the ground state structure of $Si_2Mg_9^{-1}$ with adding two magnesium atoms, the lowest energy structure of $Si_2Mg_1^{-1}1(C_1, {}^2A)$ is got. The ground state structure of Si_2Mg_{11} (C_1, ^1A) can be formed by the first metastable structure of Si_2Mg_9 with two more magnesium attracted. The lowest energy structure of $Si_2Mg_1^{+1}1(C_1, {}^2A)$ is the same as the first metastable structure of Si_2Mg_{11}, and they are quite similar as the first metastable structure of $Si_2Mg_9^{+1}$. Other metastable structures exhibit 3D cage-like structure.

Energy Difference Between Structures

As shown in **Figures 1–3**, the energy differences ΔE_1 (from -4867.41 to -4864.22 eV), ΔE_2 (from -4867.96 to -4865.96 eV), and ΔE_3 (from -4861.51 to -4857.66 eV) are quite stable and reasonable. Because the energy difference between the free neutral Si_2 and Mg_2, $E(Si_2)-E(Mg_2) = -4864.42$ eV, is quite near to the ΔE_1. In addition, $\Delta E_2 < \Delta E_1 < \Delta E_3$ is consistent with the following conclusion: if the neutral charged cluster is negatively charged, the cluster will lose energy, and if the neutral charged cluster is positively charged, the cluster will get energy. In addition, the energy differences between all metastable state structures and their corresponding ground state structures are also listed under each metastable state structure, they are all very small (from 0.01 to 2.04 eV) and reasonable.

Growth Pattern

According to the structural characteristics of the lowest energy state structures mentioned above, the growth mechanism of

TABLE 2 | The shortest bond length (Å) of Mg_{n+2}, neutral and charged $Si_2Mg_n^Q$ ($n = 1$–11; $Q = 0, \pm1$) clusters.

Clusters	The shortest bond length (Å)			Clusters	The shortest bond length (Å)
	Anionic	Cationic	Neutral		
Si_2Mg_1	$d_{Si-Si} = 5.27$	$d_{Si-Si} = 2.31$	$d_{Si-Si} = 2.21$	Mg_3	$d_{Mg-Mg} = 2.91$
	$d_{Si-Mg} = 2.63$	$d_{Si-Mg} = 2.70$	$d_{Si-Mg} = 2.54$		
Si_2Mg_2	$d_{Si-Si} = 2.37$	$d_{Si-Si} = 2.47$	$d_{Si-Si} = 2.22$	Mg_4	$d_{Mg-Mg} = 3.17$
	$d_{Si-Mg} = 2.66$	$d_{Si-Mg} = 2.66$	$d_{Si-Mg} = 2.79$		
	$d_{Mg-Mg} = 4.76$	$d_{Mg-Mg} = 2.99$	$d_{Mg-Mg} = 5.13$		
Si_2Mg_3	$d_{Si-Si} = 2.25$	$d_{Si-Si} = 2.21$	$d_{Si-Si} = 2.32$	Mg_5	$d_{Mg-Mg} = 3.45$
	$d_{Si-Mg} = 2.67$	$d_{Si-Mg} = 2.66$	$d_{Si-Mg} = 2.53$		
	$d_{Mg-Mg} = 3.01$	$d_{Mg-Mg} = 2.96$	$d_{Mg-Mg} = 3.00$		
Si_2Mg_4	$d_{Si-Si} = 2.23$	$d_{Si-Si} = 2.75$	$d_{Si-Si} = 2.27$	Mg_6	$d_{Mg-Mg} = 3.00$
	$d_{Si-Mg} = 2.77$	$d_{Si-Mg} = 2.59$	$d_{Si-Mg} = 2.68$		
	$d_{Mg-Mg} = 3.03$	$d_{Mg-Mg} = 2.99$	$d_{Mg-Mg} = 2.93$		
Si_2Mg_5	$d_{Si-Si} = 2.32$	$d_{Si-Si} = 2.59$	$d_{Si-Si} = 2.22$	Mg_7	$d_{Mg-Mg} = 3.15$
	$d_{Si-Mg} = 2.69$	$d_{Si-Mg} = 2.58$	$d_{Si-Mg} = 2.60$		
	$d_{Mg-Mg} = 3.05$	$d_{Mg-Mg} = 2.98$	$d_{Mg-Mg} = 2.88$		
Si_2Mg_6	$d_{Si-Si} = 2.33$	$d_{Si-Si} = 2.56$	$d_{Si-Si} = 2.74$	Mg_8	$d_{Mg-Mg} = 3.14$
	$d_{Si-Mg} = 2.65$	$d_{Si-Mg} = 2.64$	$d_{Si-Mg} = 2.60$		
	$d_{Mg-Mg} = 2.99$	$d_{Mg-Mg} = 2.99$	$d_{Mg-Mg} = 2.87$		
Si_2Mg_7	$d_{Si-Si} = 2.29$	$d_{Si-Si} = 2.36$	$d_{Si-Si} = 2.23$	Mg_9	$d_{Mg-Mg} = 3.12$
	$d_{Si-Mg} = 2.67$	$d_{Si-Mg} = 2.67$	$d_{Si-Mg} = 2.66$		
	$d_{Mg-Mg} = 3.03$	$d_{Mg-Mg} = 3.02$	$d_{Mg-Mg} = 2.90$		
Si_2Mg_8	$d_{Si-Si} = 2.39$	$d_{Si-Si} = 2.69$	$d_{Si-Si} = 5.15$	Mg_{10}	$d_{Mg-Mg} = 3.04$
	$d_{Si-Mg} = 2.67$	$d_{Si-Mg} = 2.65$	$d_{Si-Mg} = 2.54$		
	$d_{Mg-Mg} = 3.01$	$d_{Mg-Mg} = 2.99$	$d_{Mg-Mg} = 2.89$		
Si_2Mg_9	$d_{Si-Si} = 5.02$	$d_{Si-Si} = 2.39$	$d_{Si-Si} = 5.72$	Mg_{11}	$d_{Mg-Mg} = 3.08$
	$d_{Si-Mg} = 2.64$	$d_{Si-Mg} = 2.65$	$d_{Si-Mg} = 2.58$		
	$d_{Mg-Mg} = 2.98$	$d_{Mg-Mg} = 3.03$	$d_{Mg-Mg} = 2.92$		
Si_2Mg_{10}	$d_{Si-Si} = 5.90$	$d_{Si-Si} = 2.45$	$d_{Si-Si} = 5.84$	Mg_{12}	$d_{Mg-Mg} = 3.09$
	$d_{Si-Mg} = 2.64$	$d_{Si-Mg} = 2.67$	$d_{Si-Mg} = 2.55$		
	$d_{Mg-Mg} = 3.03$	$d_{Mg-Mg} = 3.02$	$d_{Mg-Mg} = 2.88$		
Si_2Mg_{11}	$d_{Si-Si} = 5.17$	$d_{Si-Si} = 5.22$	$d_{Si-Si} = 6.04$	Mg_{13}	$d_{Mg-Mg} = 3.03$
	$d_{Si-Mg} = 2.64$	$d_{Si-Mg} = 2.67$	$d_{Si-Mg} = 2.68$		
	$d_{Mg-Mg} = 2.96$	$d_{Mg-Mg} = 2.96$	$d_{Mg-Mg} = 2.93$		

$Si_2Mg_n^Q$ ($n = 1–11$; $Q = 0, \pm1$) clusters of silicon-magnesium sensor material can be summarized as following: (i) The lowest energy state $Si_2Mg_n^Q$ clusters favor 3D and low spin multiplicity for $n = 4–11$. (ii) Compared with neutral Si_2Mg_n clusters, charged $Si_2Mg_n^{\pm1}$ clusters formed when they get or lose electrons will change their structures in most cases. (iii) Larger size clusters $Si_2Mg_n^{0\pm1}$ show cage-like geometries, but silicon atoms are not in the center of the cage, but tend to the edge, which is different from some reports (Zhang et al., 2015). This may be related to the distribution of electrons outside the nucleus of magnesium and silicon atoms. Through the above structure optimization, we can find that the shortest chemical bond length of clusters tends to be smaller when silicon doped with magnesium. **Table 2** shows the shortest chemical bond lengths of Mg-Mg, Si-Si, Si-Mg for all Si_2Mg_n

clusters as the number of magnesium atoms increases. For comparison, **Table 2** also lists the shortest chemical bond lengths of Mg-Mg clusters with corresponding atomic numbers of pure magnesium clusters. From **Table 2**, it can be seen clearly that silicon doping into magnesium can indeed make the cluster structure more compact when the total number of atoms is the same.

The Relative Stabilities of $Si_2Mg_n^Q$($n = 1–11$; $Q = 0, \pm1$) Clusters of Silicon-Magnesium Sensor Material

In order to study the relativity stabilities of neutral and charged $Si_2Mg_n^Q$ ($n = 1–11$; $Q = 0, \pm1$) clusters of silicon-magnesium sensor material, the average binding energy E_b, fragmentation energy E_f, the second-order energy differences Δ_2E, and the
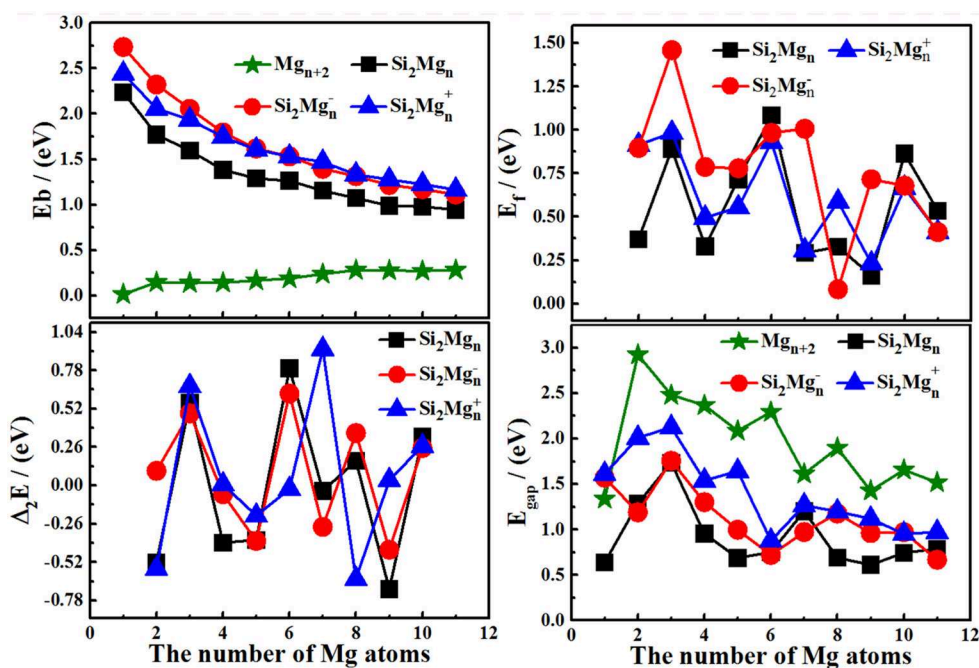
FIGURE 4 | The size-dependent properties of E_b, Δ_2E, E_f, and E_{gap} of the lowest-energy $Si_2Mg_n^Q$($n = 1–11$; $Q = 0, \pm1$) clusters of silicon-magnesium sensor material.

TABLE 3 | NCP of the lowest-energy structures for neutral $SiMg_n$ ($n = 1–11$) clusters of silicon-magnesium sensor material.

Clusters/Atom	Si-1	Si-2	Mg-1	Mg-2	Mg-3	Mg-4	Mg-5	Mg-6	Mg-7	Mg-8	Mg-9	Mg-10	Mg-11
Si_2Mg_1	−0.36	−0.36	0.72										
Si_2Mg_2	−0.55	−0.55	0.55	0.55									
Si_2Mg_3	−0.88	−0.89	0.45	0.45	0.86								
Si_2Mg_4	−0.59	−1.14	0.57	0.29	0.29	0.57							
Si_2Mg_5	−0.92	−0.76	0.26	0.27	0.23	0.46	0.45						
Si_2Mg_6	−0.89	−0.89	0.23	0.42	0.42	0.00	0.23	0.49					
Si_2Mg_7	−1.34	−0.68	0.43	0.22	0.15	0.45	0.52	0.00	0.25				
Si_2Mg_8	−1.89	−1.89	0.51	0.59	0.30	0.51	0.51	0.51	0.59	0.25			
Si_2Mg_9	−1.37	−1.53	0.61	0.25	0.22	0.42	0.49	0.25	0.22	−0.04	0.49		
Si_2Mg_{10}	−1.69	−1.61	0.49	0.00	0.16	0.34	0.37	0.35	0.37	0.48	0.15	0.59	
Si_2Mg_{11}	−1.70	−1.73	0.37	0.52	0.41	0.30	0.04	0.53	−0.03	0.30	0.22	0.58	0.19

HOMO-LUMO energy gap E_{gap} are calculated, which can be read as below:

$$E_b(Si_2Mg_n) = [nE_k(Mg) + 2E_k(Si) - E_k(Si_2Mg_n)]/(n+2) \quad (1)$$

$$E_b(Si_2Mg_n^{\pm1}) = [(n-1)E_k(Mg) + E_k(Mg^{\pm}) \\ + 2E_k(Si) - E_k(Si_2Mg_n^{\pm1})]/(n+2) \quad (2)$$

$$E_f(Si_2Mg_n^{0,\pm1}) = E_k(Si_2Mg_{n-1}^{0,\pm1}) + E_k(Mg) - E_k(Si_2Mg_n^{0,\pm1}) \quad (3)$$

$$\Delta_2E(Si_2Mg_n^{0,\pm1}) = E_k(Si_2Mg_{n-1}^{0,\pm1}) + E_k(Si_2Mg_{n+1}^{0,\pm1}) \\ - 2E_k(Si_2Mg_n^{0,\pm1}) \quad (4)$$

$$E_{gap}(Si_2Mg_n^{0,\pm1}) = E_{LUMO}(Si_2Mg_n^{0,\pm1}) - E_{HOMO}(Si_2Mg_n^{0,\pm1}) \quad (5)$$

E_k in Equations (1–4) are the total energy of the corresponding atom and ground state clusters. E_{HOMO} and E_{LUMO} in Equation (5) are the energies of highest occupied molecular orbital (HOMO) and the lowest unoccupied molecular orbital (LUMO).

The motivation for comparing pure magnesium clusters must be explained here. Physically, the most ideal (simplest) silicon doping is to replace two magnesium atoms with silicon atoms in pure magnesium clusters, and then to optimize the structure. Therefore, comparing some properties of silicon-doped magnesium clusters, we always habitually compare pure magnesium clusters with the total number of corresponding atoms in our research. The size-dependent properties of E_b, E_f, Δ_2E, and E_{gap} for the lowest energy state $Si_2Mg_n^Q$ ($n = 1$–11; $Q = 0, \pm1$) clusters of silicon-magnesium sensor material are presented in **Figure 4**. We can summarize the properties as the following:

1) The E_b values of all $Si_2Mg_n^Q$ ($n = 1$–11; $Q = 0, \pm1$) clusters of silicon-magnesium sensor material decrease followed by same tendency with the size increases, but the E_b values of pure Mg_{n+2} clusters are gradually increase. In addition, the E_b values of cationic $Si_2Mg_n^{+1}$ are always the highest, while the E_b values of neutral $Si_2Mg_n^0$ are the lowest all the time. It means that electron removal can enhance the chemical properties of Si_2Mg_n clusters.

2) The E_f curves of neutral and charged $Si_2Mg_n^Q$ ($n = 1$–11; $Q = 0, \pm1$) clusters of silicon-magnesium sensor material have a similar oscillating tendency. For neutral $Si_2Mg_n^0$ clusters, the stronger relative stability clusters are $Si_2Mg_3^0$, $Si_2Mg_6^0$, and $Si_2Mg_{10}^0$ based on the maxim of E_f values. For anionic $Si_2Mg_n^{-1}$ clusters, three significant maxima are found at $n = 3, 7, 9$, which indicate that $Si_2Mg_3^{-1}$, $Si_2Mg_7^{-1}$, and $Si_2Mg_9^{-1}$ clusters are the most stable clusters. For cationic $Si_2Mg_n^{+1}$ clusters, three local peaks can be found from the E_f curve, it

TABLE 4 | NCP of the lowest-energy structures for anionic $Si_2Mg_n^{-1}$ ($n = 1$–11) clusters of silicon-magnesium sensor material.

Clusters/Atom	Si-1	Si-2	Mg-1	Mg-2	Mg-3	Mg-4	Mg-5	Mg-6	Mg-7	Mg-8	Mg-9	Mg-10	Mg-11
$Si_2Mg_1^-$	−0.73	−0.73	0.46										
$Si_2Mg_2^-$	−0.81	−0.81	0.31	0.31									
$Si_2Mg_3^-$	−0.88	−0.88	0.38	0.19	0.19								
$Si_2Mg_4^-$	−0.65	−1.07	0.27	0.09	0.09	0.27							
$Si_2Mg_5^-$	−0.98	−0.98	0.23	0.07	0.23	0.35	0.07						
$Si_2Mg_6^-$	−0.53	−0.53	−0.07	0.08	0.08	−0.07	0.03	0.03					
$Si_2Mg_7^-$	−0.79	−1.46	0.22	0.05	0.35	0.19	0.09	−0.02	0.37				
$Si_2Mg_8^-$	−1.47	−1.49	0.30	0.27	0.17	0.39	0.19	0.21	0.17	0.26			
$Si_2Mg_9^-$	−1.52	−1.67	0.41	0.27	0.04	0.29	0.00	0.33	0.38	0.34	0.12		
$Si_2Mg_{10}^-$	−1.83	−1.74	0.46	0.05	0.02	0.31	0.30	0.31	0.30	0.38	0.02	0.43	
$Si_2Mg_{11}^-$	−1.88	−1.80	0.35	−0.19	0.44	0.45	0.04	0.09	0.04	0.43	0.49	0.30	0.25

TABLE 5 | NCP of the lowest-energy structures for cationic $Si_2Mg_n^{+1}$ ($n = 1$–11) clusters of silicon-magnesium sensor material.

Clusters/Atom	Si-1	Si-2	Mg-1	Mg-2	Mg-3	Mg-4	Mg-5	Mg-6	Mg-7	Mg-8	Mg-9	Mg-10	Mg-11
$Si_2Mg_1^+$	0.02	0.03	0.95										
$Si_2Mg_2^+$	−0.34	−0.34	0.84	0.84									
$Si_2Mg_3^+$	−0.38	−0.37	0.55	0.65	0.55								
$Si_2Mg_4^+$	−1.16	−1.16	0.99	0.99	0.67	0.67							
$Si_2Mg_5^+$	−1.37	−1.29	0.67	0.66	0.64	1.09	0.61						
$Si_2Mg_6^+$	−1.15	−1.15	0.44	0.44	0.78	0.44	0.44	0.78					
$Si_2Mg_7^+$	−1.09	−1.09	0.65	0.42	0.42	0.42	0.42	0.21	0.65				
$Si_2Mg_8^+$	−1.33	−1.14	0.35	0.49	0.85	−0.12	0.43	0.81	0.30	0.36			
$Si_2Mg_9^+$	−1.43	−1.49	0.55	0.55	0.35	0.53	0.53	0.19	0.19	0.69	0.35		
$Si_2Mg_{10}^+$	−1.51	−1.51	0.49	0.38	0.48	0.40	0.22	0.41	0.48	0.49	0.41	0.26	
$Si_2Mg_{11}^+$	−2.06	−2.06	0.12	0.45	0.59	0.66	0.52	0.52	0.59	0.28	0.28	0.45	0.66

means that $Si_2Mg_3^{+1}$, $Si_2Mg_6^{+1}$, Si_2 Mg_8^{+1} clusters are more stable than their neighbors.

3) The irregular oscillation behaviors are the most prominent feature of Δ_2E curves of all $Si_2Mg_n^Q$ (n = 1–11; Q = 0, ±1) clusters of silicon-magnesium sensor material. The maxima are found at n = 3 for all $Si_2Mg_n^Q$ clusters, n = 6 and 8 for both neutral $Si_2Mg_n^0$ and anionic $Si_2Mg_n^{-1}$ clusters, n = 7 for cationic $Si_2Mg_n^{+1}$ clusters. It means that the $Si_2Mg_3^{-1}$, $Si_2Mg_6^{-1}$, $Si_2Mg_8^{-1}$, $Si_2Mg_3^{+1}$, $Si_2Mg+1\ 6$, and $Si_2Mg_7^{+1}$ clusters have slightly stronger relative stabilities and have large abundances in mass spectroscopy in comparison with the corresponding neighbors. For neutral clusters, $Si_2Mg_3^0$, $Si_2Mg_6^0$, and $Si_2Mg_8^0$ clusters are more stable than other clusters.

4) The pure Mg_{n+2} clusters have the highest E_{gap} is an unexpected conclusion, because pure magnesium has higher chemical stability than silicon magnesium. For $Si_2Mg_n^Q$ (n = 1–11; Q = 0, ±1) clusters, the E_{gap} of cationic $Si_2Mg_n^{+1}$ clutters is always the higher one. It means that $Si_2Mg_n^{+1}$ clusters have higher chemical stability than the neutral and anionic $Si_2Mg_n^Q$ clusters. The curves of E_{gap} show that the maxima values appear at n = 3 for all $Si_2Mg_n^Q$ (Q = 0, ±1) clusters, n = 7 for both neutral $Si_2Mg_n^0$ and cationic $Si_2Mg_n^{+1}$, and n = 8 for anionic $Si_2Mg_n^{-1}$ clusters, which implies that the higher chemical stability clusters are $Si_2Mg_3^{-1}$, $Si_2Mg_3^{-1}$, $Si_2Mg_3^{+1}$, $Si_2Mg_7^0$, $Si_2Mg_7^{+1}$, and $Si_2Mg_8^{-1}$.

Based on the discussions about E_b, E_f, Δ_2E, and E_{gap}, we can conclude that the magic numbers of neutral and charged $Si_2Mg_n^Q$ (n = 1–11; Q = 0, ±1) clusters of silicon-magnesium sensor material are $Si_2Mg_3^0$, $Si_2Mg_3^{-1}$, $Si_2Mg_3^{+1}$.

The Charge Transfer of $Si_2Mg_n^Q$(n = 1–11; Q = 0, ±1) Clusters of Silicon-Magnesium Sensor Material

Natural charge population (NCP) and natural electron population (NEC) of clusters are two important parameters to study the localization of charges in clusters (Trivedi et al., 2014). In order to study internal charge transfer of neutral and charged $Si_2Mg_n^Q$ (n = 1–11; Q = 0, ±1) clusters of silicon-magnesium sensor material, we calculate NCP and NEC for the ground state structures of $Si_2Mg_n^Q$ (n = 1–11; Q = 0, ±1), and the results are summarized in the **Tables 3–6**. We can find that the charges of silicon atoms in $Si_2Mg_n^Q$ (n = 1–11; Q = 0, ±1) clusters is very significant from the **Tables 3–5**. Specifically, except for $Si_2Mg_1^{+1}$, silicon atoms are negatively charged in the range of −0.34 to −2.06 electrons, and most magnesium atoms are positively charged in the range of 0.02–0.99 electrons. This result is consistent with expectation, because electrons are always transferred from magnesium atoms to silicon atoms in $Si_2Mg_n^Q$ clusters. In short, the NCP of Si atoms indicates that silicon atoms are electron acceptors in $Si_2Mg_n^Q$ clusters. The NEC of silicon atoms can be found in the **Table 6**, the electronic configuration for silicon atoms ($3s^13p^3$) shows that 3p orbital get

TABLE 7 | AIP, VIP, AEA, VEA of ground state $Si_2Mg_n^Q$ (n = 1–11; Q = 0, ±1) clusters of silicon-magnesium sensor material.

n	AIP (eV)	VIP (eV)	|AIP-VIP| (eV)	AEA (eV)	VEA (eV)	|AEA-VEA| (eV)	|VIP-VEA| (eV)
1	7.11	7.04	0.07	1.44	0.91	0.53	6.13
2	6.59	6.33	0.25	1.61	1.24	0.37	5.09
3	6.02	6.37	0.36	1.70	1.59	0.11	4.78
4	5.56	5.92	0.36	1.87	1.78	0.08	4.14
5	5.50	5.68	0.18	1.71	1.20	0.50	4.48
6	5.60	5.79	0.19	1.55	1.21	0.34	4.58
7	4.88	5.57	0.69	1.57	1.34	0.23	4.23
8	5.13	5.42	0.29	1.83	1.36	0.47	4.06
9	4.57	5.34	0.77	1.90	1.66	0.24	3.68
10	4.76	5.32	0.57	1.70	1.52	0.18	3.80
11	4.88	5.03	0.15	1.58	1.40	0.18	3.63

TABLE 6 | NEC of the lowest-energy structures for neutral and charged $Si_2Mg_n^Q$(n = 1–11; Q = 0, ±1) clusters of silicon-magnesium sensor material.

Clusters	Neutral		Anionic		Cationic	
	Si-1	Si-2	Si-1	Si-2	Si-1	Si-2
Si_2Mg_1	$3s^{1.75}3p^{2.60}$	$3s^{1.75}3p^{2.59}$	$3s^{1.89}3p^{2.83}$	$3s^{1.89}3p^{2.83}$	$3s^{1.85}3p^{2.11}$	$3s^{1.85}3p^{2.10}$
Si_2Mg_2	$3s^{1.76}3p^{2.77}$	$3s^{1.76}3p^{2.77}$	$3s^{1.71}3p^{3.07}$	$3s^{1.71}3p^{3.07}$	$3s^{1.81}3p^{2.51}$	$3s^{1.81}3p^{2.51}$
Si_2Mg_3	$3s^{1.68}3p^{3.19.}$	$3s^{1.67}3p^{3.19}$	$3s^{1.65}3p^{3.21}$	$3s^{1.65}3p^{3.21}$	$3s^{1.73}3p^{2.62}$	$3s^{1.73}3p^{2.62}$
Si_2Mg_4	$3s^{1.69}3p^{2.88.}$	$3s^{1.63}3p^{3.48}$	$3s^{1.66}3p^{2.96}$	$3s^{1.59}3p^{3.45}$	$3s^{1.74}3p^{3.40}$	$3s^{1.74}3p^{3.40}$
Si_2Mg_5	$3s^{1.59}3p^{3.311}$	$3s^{1.62}3p^{3.11}$	$3s^{1.62}3p^{3.32}$	$3s^{1.62}3p^{3.32}$	$3s^{1.71}3p^{3.64}$	$3s^{1.72}3p^{3.55}$
Si_2Mg_6	$3s^{1.61}3p^{3.25}$	$3s^{1.61}3p^{3.25}$	$3s^{1.59}3p^{3.39}$	$3s^{1.59}3p^{3.39}$	$3s^{1.67}3p^{3.45}$	$3s^{1.67}3p^{3.45}$
Si_2Mg_7	$3s^{1.54}3p^{3.76}$	$3s^{1.62}3p^{3.03}$	$3s^{1.59}3p^{3.17}$	$3s^{1.53}3p^{3.89}$	$3s^{1.61}3p^{3.44}$	$3s^{1.61}3p^{3.44}$
Si_2Mg_8	$3s^{1.64}3p^{4.24}$	$3s^{1.64}3p^{4.24}$	$3s^{1.60}3p^{3.83}$	$3s^{1.59}3p^{3.85}$	$3s^{1.62}3p^{3.68}$	$3s^{1.65}3p^{3.46}$
Si_2Mg_9	$3s^{1.63}3p^{3.72}$	$3s^{1.60}3p^{3.92}$	$3s^{1.62}3p^{3.88}$	$3s^{1.59}3p^{4.07}$	$3s^{1.60}3p^{3.80}$	$3s^{1.56}3p^{3.89}$
Si_2Mg_{10}	$3s^{1.59}3p^{4.09}$	$3s^{1.62}3p^{3.98}$	$3s^{1.60}3p^{4.21}$	$3s^{1.61}3p^{4.11}$	$3s^{1.60}3p^{3.87}$	$3s^{1.60}3p^{3.87}$
Si_2Mg_{11}	$3s^{1.61}3p^{4.08}$	$3s^{1.59}3p^{4.13}$	$3s^{1.59}3p^{4.28}$	$3s^{1.58}3p^{4.21}$	$3s^{1.61}3p^{4.43}$	$3s^{1.61}3p^{4.43}$

0.10–2.28 electrons, while 3s orbital loses 0.11–0.47 electrons. Obviously, charge transfer occurs only in the outermost electron orbit, and strong s-p hybridizations are presented in silicon atoms of $Si_2Mg_n^Q$ clusters. Notably, the contributions of 4s and 5d orbitals are almost zero and can be ignored. Moreover, the charges of 3s and 3p orbitals for two silicon atoms in the ground state of $Si_2Mg_n^Q$ clusters are equal except for $Si_2Mg_{3-5}^-$, $Si_2Mg_7^-$, $Si_2Mg_{9-11}^-$ $Si_2Mg_4^-$, $Si_2Mg_{7-11}^-$, $Si_2Mg_5^+$, and $Si_2Mg_{8-9}^+$.

Ionization Potential and Electron Affinity of $Si_2Mg_n^Q$ ($n = 1–11$; $Q = 0, ±1$) Clusters of Silicon-Magnesium Sensor Material

Adiabatic ionization potential (AIP), vertical ionization potential (VIP), adiabatic electron affinity (AEA), and vertical electron affinity (VEA) are important characteristics of the electronic properties for clusters. On the basis of optimizing the structure, AIP, VIP, AEA, and VEA are calculated and listed in the **Table 7** with the following formulas (Deka et al., 2014):

$$AIP = E_{(optimized\ cation)} - E_{(optimized\ neutral)} \quad (6)$$

$$VIP = E_{(cation\ at\ optimized\ neutral\ geometry)} - E_{(optimized\ neutral)} \quad (7)$$

$$AEA = E_{(optimized\ neutral)} - E_{(optimized\ anion)} \quad (8)$$

$$VEA = E_{(optimized\ neutral)} - E_{(anion\ at\ optimized\ neutral\ geometry)} \quad (9)$$

It should be pointed out that the properties of neutral clusters are related to the values of VIP and VEA, while the properties of anionic and cationic clusters are related to AEA and AIP. **Figures 5A,B** show the size dependence of the AIP, VIP, AEA, and VEA. As **Figure 5A** showed, the curves of AIP and VIP have the same tendencies as the cluster size increases except $n = 3, 8, 10$. This result means that most cations are similar to the corresponding neutrals. In addition, from the **Table 7**, we can find that except for $n = 3, 4, 7, 9, 10$, the |AIP-VIP| values are in the range of 0.07–0.29 eV, which implies that the deformation of these structures corresponding to their neutral clusters are not big. The relation between AEA and VEA is showed in the **Figure 5B**, one can find that they also have the same tendencies and the |AEA-VEA| values are all small except for $n = 1, 2, 5, 6$, and 8, which means that these structures of $Si_2Mg_n^{-1}$ clusters do not differ greatly from the corresponding Si_2Mg_n clusters. In addition, as one knows that |VIP-VEA| can present the chemical hardness and is always used to characterize the stability of clusters (Pearson, 1997). **Table 7** also shows the hardness of Si_2Mg_n ($n= 1–11$) clusters, and one can find that the hardness of Si_2Mg_n clusters decreases with the increase of magnesium atoms. It is noteworthy that when $n = 6$, the hardness of the corresponding clusters is obviously larger than that of the adjacent clusters, which indicates that the stability of Si_2Mg_6 is higher. This conclusion is consistent with that of the Δ_2E in **Figure 4**.
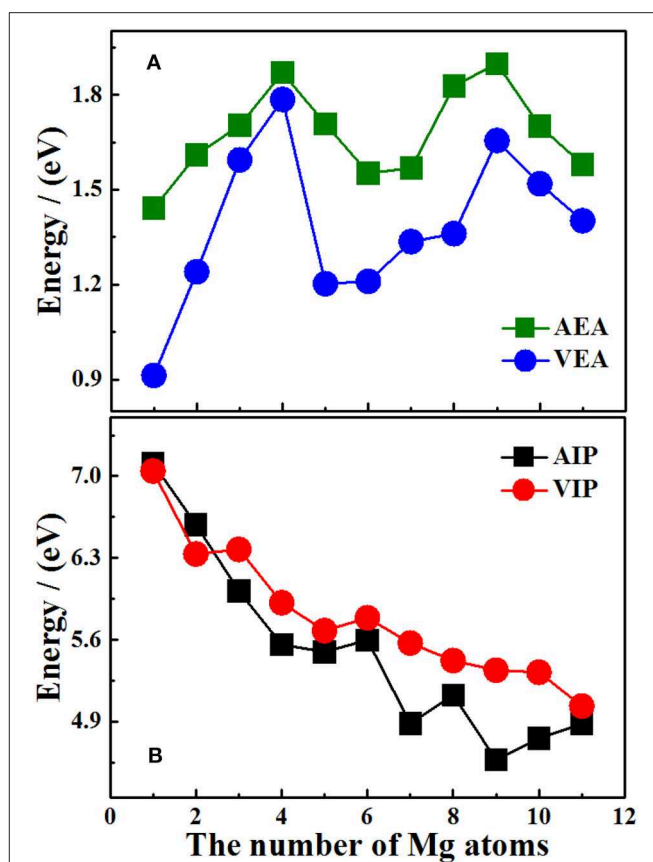
FIGURE 5 | Size dependence of AIP, VIP, AEA, and VEA of ground state $Si_2Mg_n^Q$ ($n = 1–11$; $Q =0, ±1$) clusters of silicon-magnesium sensor material. **(A)** Size dependent properties of AEA and VEA of the ground state of $Si_2Mg_n^Q$ ($Q = 0, ±1$; $n = 1–11$) clusters. **(B)** Size dependent properties of AIP and VIP of the ground state of $Si_2Mg_n^Q$($Q = 0, ±1$; $n = 1–11$) clusters.

Infrared and Raman Spectra of $Si_2Mg_n^Q$ ($n = 1–11$; $Q = 0, ±1$) Clusters of Silicon-Magnesium Sensor Material

In order to further determine the stability of silicon-magnesium semiconductor sensor material, we calculate the infrared and Raman spectra of ground state of pure Mg_{n+2} and all $Si_2Mg_n^Q$ ($n = 1–11$; $Q = 0, ±1$) clusters at B3LYP/6-311G (d) level, and present them in **Figures 6–9**. **Figure 6** presents the infrared spectra of the lowest energy structure of Mg_{n+2} ($n = 1–11$) and $Si_2Mg_n^Q$ ($n = 1–5$; $Q = 0, ±1$) clusters. It is necessary to point out that the vibration spectra (intensity ratio, line width, wave number, and location) are related to the calculation methods and basis groups. For example, the IR spectra of Mg_{2-31} clusters are calculated and showed by two different basis sets under B3PW1 function (Belyaev et al., 2016), but the overall trend of the spectra is similar. By our calculation, the main absorption bands of Mg_{n+2} clusters ($n = 1–11$) are located at 60–230 cm^{-1}, which is similar as the results of the existing report (Belyaev et al., 2016). From **Figures 6, 7**, one can find that the IR strong peaks frequencies are in the range of 40–500 cm^{-1} for neutral $Si_2Mg_n^0$ clusters, 80–460 cm^{-1} for anionic $Si_2Mg_n^{-1}$ clusters and
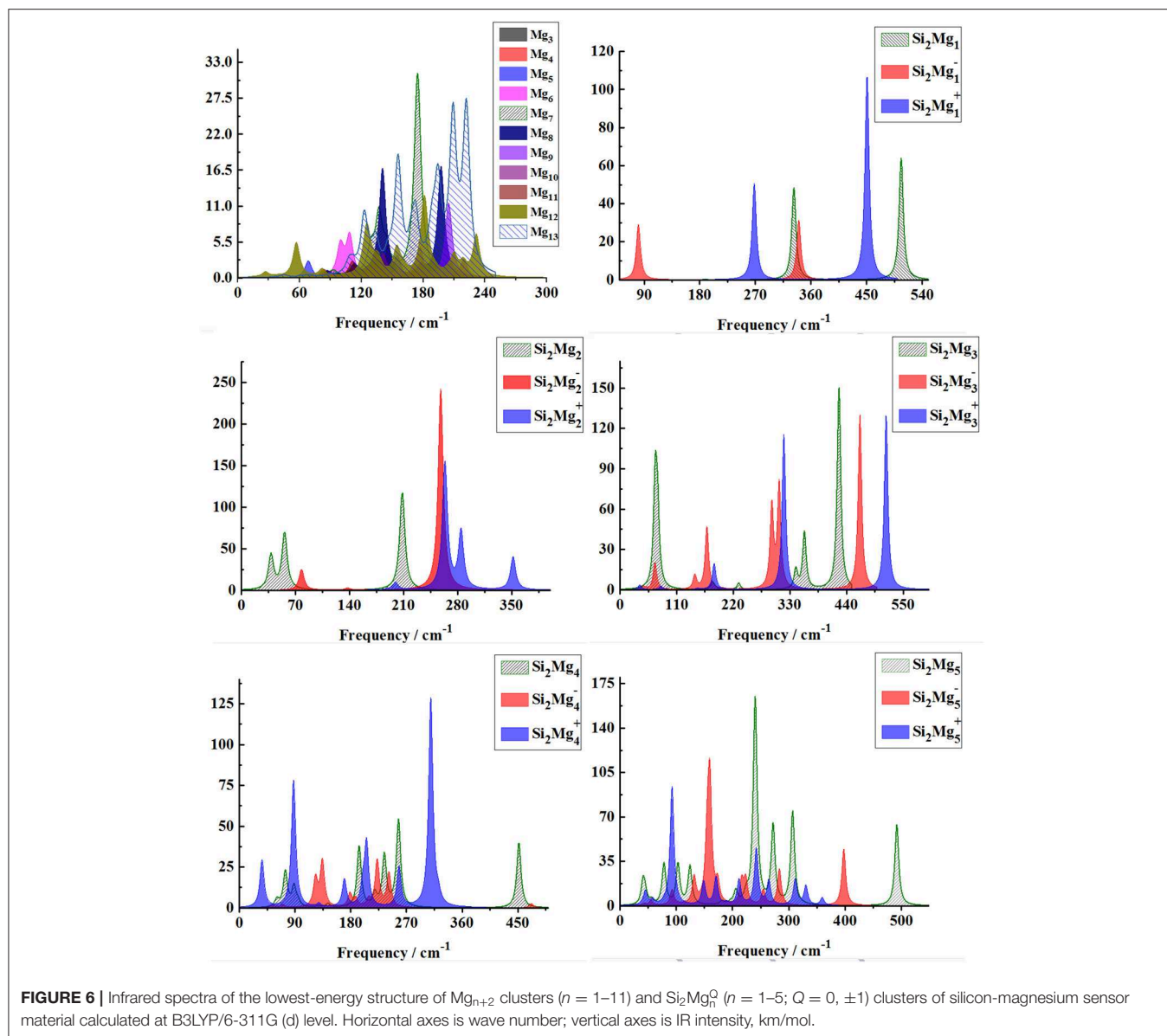
FIGURE 6 | Infrared spectra of the lowest-energy structure of Mg_{n+2} clusters ($n = 1$–11) and $Si_2Mg_n^Q$ ($n = 1$–5; $Q = 0, \pm 1$) clusters of silicon-magnesium sensor material calculated at B3LYP/6-311G (d) level. Horizontal axes is wave number; vertical axes is IR intensity, km/mol.

30–540 cm^{-1}. In small size (n $\leq$ 5) clusters, the IR strong vibration spectra of neutral, anionic and cationic $Si_2Mg_n^Q$($n =$ 1–11; $Q = 0, \pm 1$) clusters are easily distinguished from each other. While, in large size ($n =$ 6–11) clusters, the frequency of IR strong vibration spectra of these clusters is relatively close from mid-frequency to the high-frequency region. As we know that the electron-absorbing base moves the infrared absorption peak to the high frequency region, and the electron-supplying base moves the infrared absorption peak to the low frequency region. In addition, the tension property of materials shows that the larger the tension of structures, the higher the infrared absorption frequency. Therefore, we can find that two interesting conclusions from **Figures 6**, **7**. (i) The electron-absorbing base structure of neutral cluster materials is stronger than that of charged clusters, and this trend decreases with the increase

of the number of magnesium atoms. (ii) With the increase of magnesium atoms around silicon atoms, the peak infrared absorption frequency shifts from relative high frequency to relative low frequency. This indicates that the tension properties of cluster materials with high Mg atoms are not good. The vibration modes of IR spectra of $Si_2Mg_n^Q$($n =$ 1–11; $Q = 0, \pm 1$) clusters are very numerous and complex, and as the results discussed above show that magic number clusters of $Si_2Mg_3^0$, $Si_2Mg_3^{-1}$, $Si_2Mg_3^{+1}$ are more stable than other clusters. Therefore, here we only focus on these three clusters' vibration modes. As **Figure 6** showed, the highest intensity IR frequency of neutral $Si_2Mg_3^0$ locates at 425.28 cm^{-1}, and its vibration mode is assigned as stretching of Si2-Si1 bond. The frequency of the strongest peak of anionic $Si_2Mg_3^{-1}$ cluster at 465.87 cm^{-1}, and its vibrational mode is as the same as the highest peak of neutral $Si_2Mg_3^0$. The
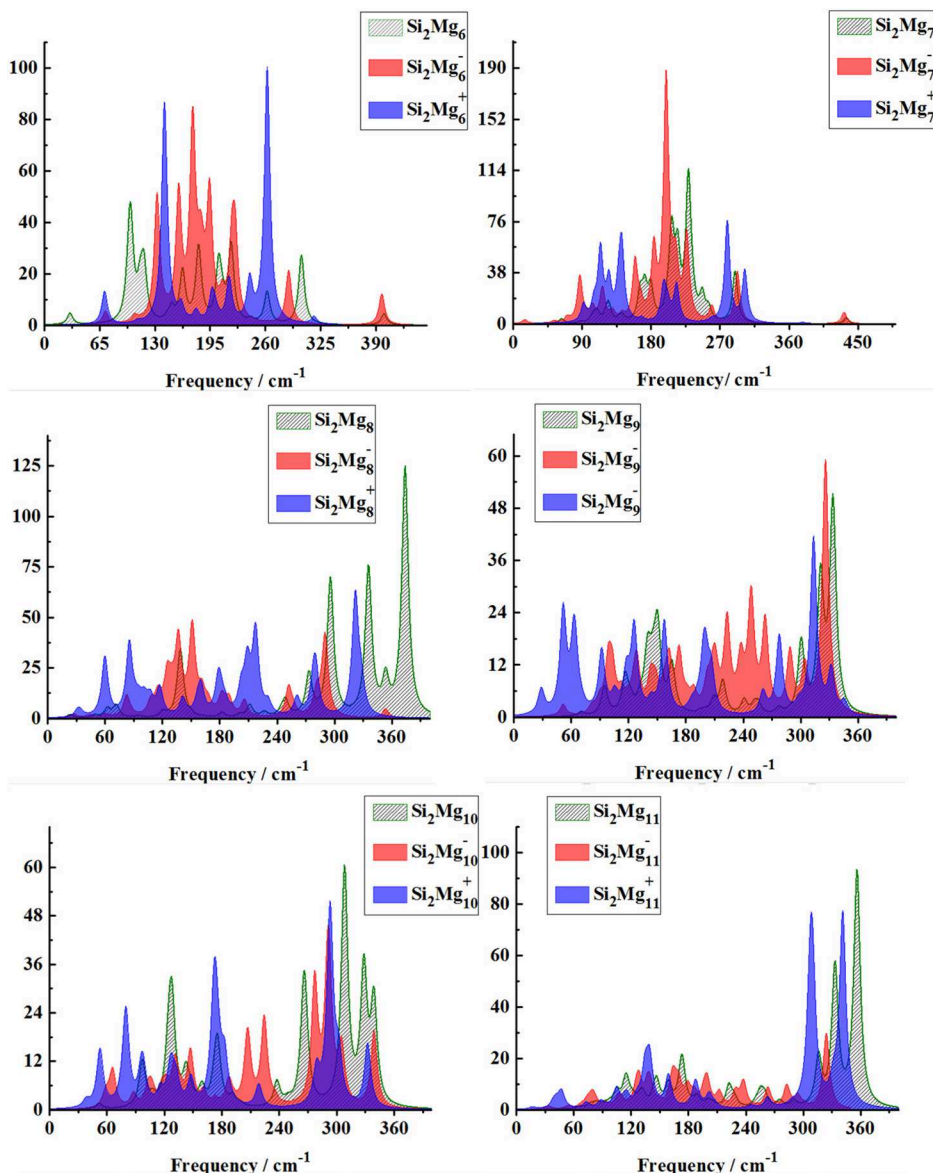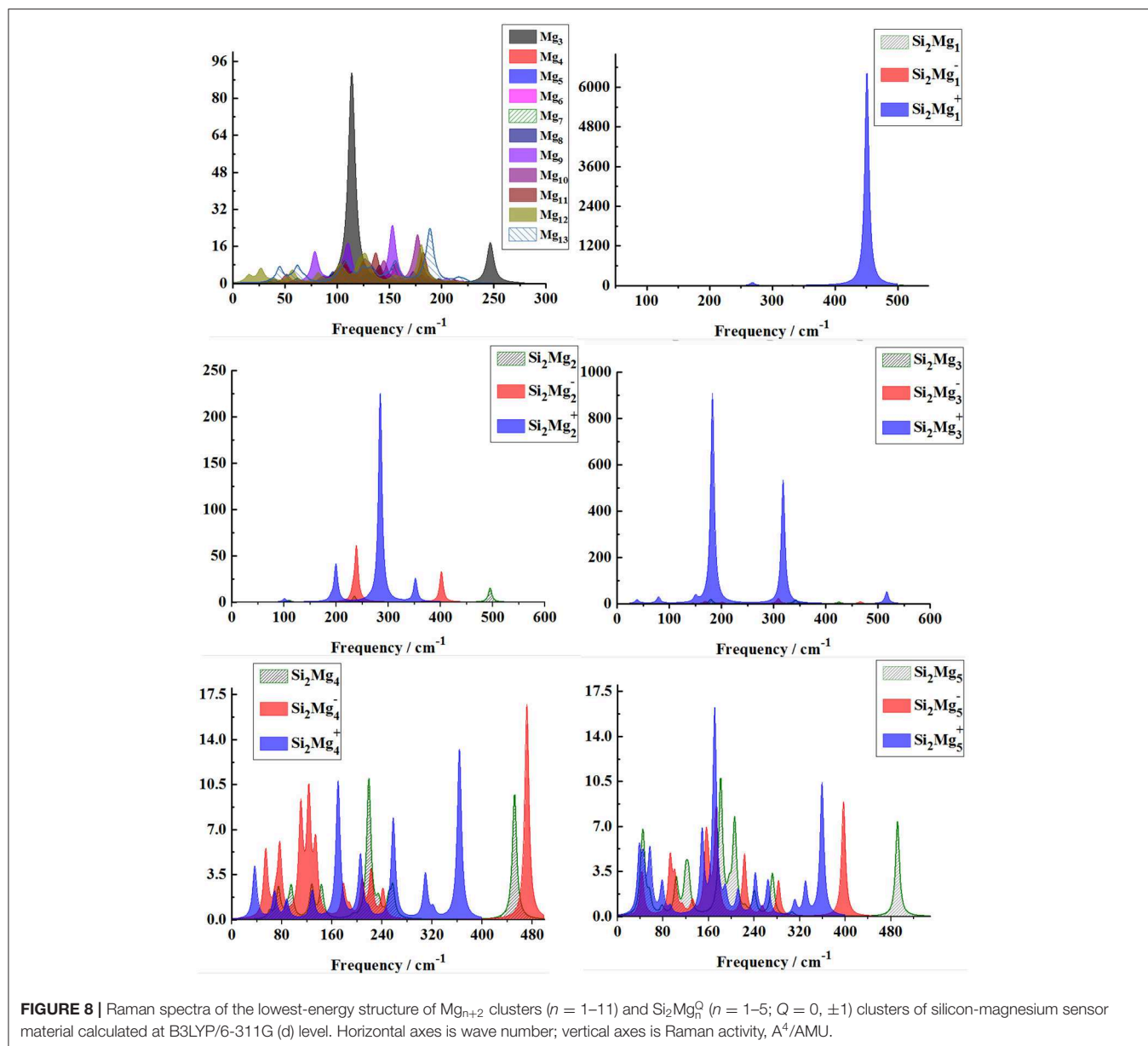
FIGURE 7 | Infrared spectra of the lowest-energy structure of $Si_2Mg_n^Q$ ($n = 6$–11; $Q = 0, \pm1$) clusters of silicon-magnesium sensor material calculated at B3LYP/6-311G (d) level. Horizontal axes is wave number; vertical axes is IR intensity, km/mol.

strong peaks of IR spectra of cationic $Si_2Mg_3^{+1}$ cluster at 516.55 cm^{-1} resulted from the stretching of Si2-Si1 bond.

From **Figures 8**, **9**, one can find Raman spectra of Mg_{n+2} and $Si_2Mg_n^Q$ ($n = 1$–11; $Q = 0, \pm1$) clusters. Raman spectra activity of Mg_{n+2} ($n = 1$–11) clusters show a fairly low frequency (in the range of 25–180 cm^{-1}) nature except for Mg_3. Raman spectra activity properties of $Si_2Mg_n^Q$ ($n = 1$–11; $Q = 0, \pm1$) clusters are rather different from their IR absorption properties. In small size clusters ($n = 1$–3), the Raman activity of cationic $Si_2Mg_n^Q$ clusters is fairly high in Mid-frequency and high-frequency regions. When $n = 4, 5$, the Raman activity of the clusters is widely distributed, and it is easy to distinguish them from each other. However, after $n > 5$, the Raman activity of the clusters begin to

shift slowly from the high-frequency region to the mid-frequency region and close to each other. The Raman activity frequency of $Si_2Mg_n^Q$ ($Q = 0, \pm1$) clusters are 50–480 cm^{-1} for neutral $Si_2Mg_n^0$, 40–480 cm^{-1} for anionic $Si_2Mg_n^{-1}$ and 40–450 cm^{-1}, respectively. When studying the vibration information of Raman spectra with specific magic number structure, we can find that the maximum Raman activity of neutral $Si_2Mg_3^0$ cluster at the frequency of 179.66 cm^{-1} with the stretching of Mg3-Mg4 bond, the frequency of the highest peak of anionic $Si_2Mg_3^{-1}$ cluster at 308.76 cm^{-1} is assigned as stretching of Si1-Mg3 and Si2-Mg3 bonds and the highest Raman activity frequency peak of cationic $Si_2Mg_3^{+1}$ cluster at 182.25 cm^{-1} vibrated as stretching of Si1-Mg4, Si2-Mg4 bonds.

FIGURE 8 | Raman spectra of the lowest-energy structure of Mg_{n+2} clusters ($n = 1–11$) and $Si_2Mg_n^Q$ ($n = 1–5$; $Q = 0, \pm1$) clusters of silicon-magnesium sensor material calculated at B3LYP/6-311G (d) level. Horizontal axes is wave number; vertical axes is Raman activity, A^4/AMU.

CONCLUSION

The structural, stability, electronic structure and spectral properties of silicon-magnesium semiconductor sensor materials are systematically studied by $Si_2Mg_n^Q$ ($n = 1–11$; $Q = 0, \pm1$) clusters in this paper. By using the CALYPSO searching method and B3LYP at 6-311G (d) basis set of DFT, the results can be summarized below:

(i) The results of $Si_2Mg_n^Q$ ($n = 1–11$; $Q = 0, \pm1$) clusters' structure of silicon-magnesium semiconductor sensor material reveal that only a few of the lowest-energy anionic and cationic geometries are similar as their corresponding neutral ones, most of them are deformation. This conclusion is in good agreement with the changes of

their AIP, VIP, AEA, and VEA. |VIP-VEA| values reveal that the hardness of Si_2Mg_n clusters decreases with the increase of magnesium atoms.

(ii) For the stability of $Si_2Mg_n^Q$ ($n = 1–11$; $Q = 0, \pm1$) clusters of silicon-magnesium semiconductor sensor materials, the average bonding energy of neutral $Si_2Mg_n^0$ clusters are always smaller than the anionic and cationic ones show that attachment or detachment of one electron can enhance chemical stabilities of $Si_2Mg_n^0$ clusters. Based on the calculations of E_b, E_f, Δ_2E, and E_{gap}, we find that $Si_2Mg_3^0$, $Si_2Mg_3^{-1}$, $Si_2Mg_3^{+1}$, clusters have stronger stabilities than other clusters.

(iii) The cluster electronic structure of silicon-magnesium semiconductor sensor materials is analyzed. The results of
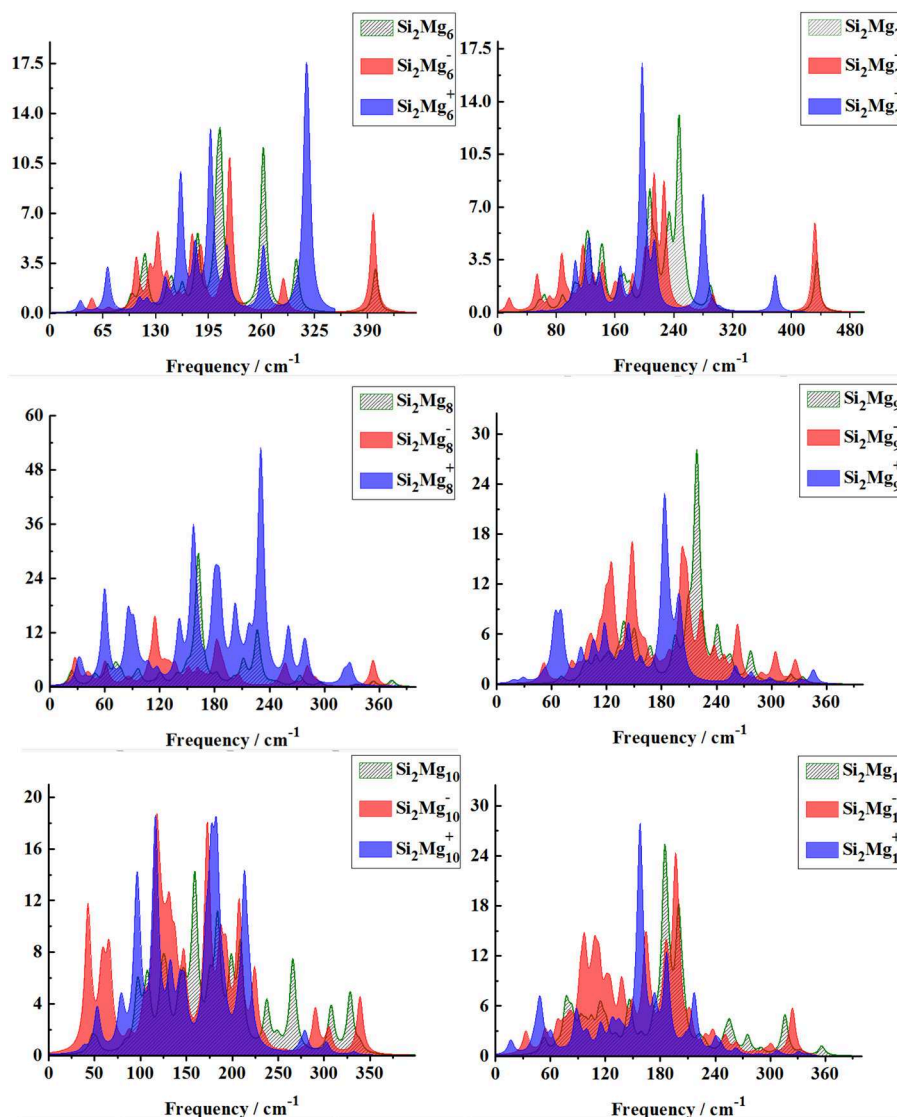
FIGURE 9 | Raman spectra of the lowest-energy structure of $Si_2Mg_n^Q$ ($n = 6$–11; $Q = 0, \pm1$) clusters of silicon-magnesium sensor material calculated at B3LYP/6-311G (d) level. Horizontal axes is wave number; vertical axes is Raman activity, A^4/AMU.

NCP and NEC show that the charges in $Si_2Mg_n^Q$ ($n = 1$–11; $Q = 0, \pm1$) clusters transfer from Mg atoms to Si atoms, and the sp hybridization is existed in Si atoms in the clusters.

(iv) The infrared (IR) and Raman spectra of $Si_2Mg_n^Q$ ($n = 1$–11; $Q = 0, \pm1$) clusters of silicon-magnesium semiconductor sensor materials show different properties. Both IR and Raman spectra can be easily distinguished each other in small size clusters, however, in large clusters, IR spectra converge and concentrate at high frequencies, while Raman spectra converge and concentrate at mid-frequency region.

DATA AVAILABILITY STATEMENT

All datasets generated for this study are included in the article/supplementary material.

AUTHOR CONTRIBUTIONS

All authors listed have made a substantial, direct and intellectual contribution to the work, and approved it for publication.

FUNDING

REFERENCES

Atanassov, A., and Baleva, M. (2007). On the band diagram of Mg_2Si/Si heterojunction as deduced from optical constants dispersions. *Thin Solid Films* 515, 3046–3051. doi: 10.1016/j.tsf.2006.08.015

Aymerich, F., and Mula, G. (2010). Pseudopotential band structures of Mg_2Si, Mg_2Ge, Mg_2Sn, and of the solid solution $Mg_2(Ge, Sn)$. *Phys. Status Solidi* 42, 697–704. doi: 10.1002/pssb.19700420224

Belyaev, S. N., Panteleev, S. V., Ignatov, S. K., and Razuvaev, A. G. (2016). Structural, electronic, thermodynamic and spectral properties of Mg_n (n = 2-31) clusters. A DFT study. *Comput. Theor. Chem.* 1079, 34–46. doi: 10.1016/j.comptc.2016.01.011

Boher, P., Houdy, P., Kühne, M., Müller, P., Barchewitz, R., and Delaboudiniere, J. P., et al. (1992). Tungsten/magnesium silicide multilayers for soft x-ray optics. *J. Xray. Sci. Technol.* 3, 118–132. doi: 10.1016/0895-3996(92)90004-4

Bole, C., Weiguo, S., Xiao-Yu, K., Cheng, L., Xinxin, X., Hongxiao, S., et al. (2018). Structural stability and evolution of medium-sized tantalum-doped boron clusters: a half-sandwich-structured tab12– cluster. *Inorg. Chem.* 57, 343–350. doi: 10.1021/acs.inorgchem.7b02585

Chen, Q., Xie, Q., Zhao, F., Cui, D., and Li, X. (2010). First-principles calculations of electronic structure and optical properties of strained Mg_2Si. *Chin. Sci. Bull.* 55, 2236–2242. doi: 10.1007/s11434-010-3280-7

de Heer, W. A., Knight, W. D., Chou, M. Y., and Cohen, M. L. (1987). Electronic shell structure and metal clusters. *Solid State Phys.* 40. 93–181. doi: 10.1016/S0081-1947(08)60691-8

Deka, R. C., Bhattacharjee, D., Chakrabartty, A. K., and Mishra, B. K. (2014). Catalytic oxidation of NO by Au_2^- dimers: a DFT study. *RSC Adv.* 4, 5399–5404. doi: 10.1039/c3ra42240b

Dmytruk, A., Dmitruk, I., Blonskyy, I., Belosludov, R., Kawazoe, Y., and Kasuya, A. (2009). ZnO clusters: laser ablation production and time-of-flight mass spectroscopic study. *Microelectron. J.* 40, 218–220. doi: 10.1016/j.mejo.2008.07.010

Frisch, M., Trucks, G., Schlegel, H., Scuseria, G., Robb, M., Cheeseman, J., et al. (2014). *Gaussian 09*. Wallingford, CT: Gaussian, Inc., 481.

Huber, K. P. (1979). "Constants of diatomic molecules," in *Molecular Spectra and Molecular Structure*.

Imai, Y., Watanabe, A., and Mukaida, M. (2003). Electronic structures of semiconducting alkaline-earth metal silicides. *J. Alloys Comp.* 358, 257–263. doi: 10.1016/S0925-8388(03)00037-9

Jin, Y., Maroulis, G., Kuang, X., Ding, L., Lu, C., Wang, J., et al. (2015a). Geometries, stabilities and fragmental channels of neutral and charged sulfur clusters: Sn(q) (n = 3-20, q = 0, Â±1). *Phys. Chem. Chem. Phys.* 17, 13590–13597. doi: 10.1039/C5CP00728C

Jin, Y., Tian, Y., Kuang, X., Zhang, C., Lu, C., Wang, J., et al. (2015b). Ab initio search for global minimum structures of pure and boron doped silver clusters. *J. Phys. Chem. A* 119, 6738–6745. doi: 10.1021/acs.jpca.5b03542

Ju, M., Lv, J., Kuang, X. Y., Ding, L. P., Lu, C., Wang, J. J., et al. (2015). Systematic theoretical investigation of geometries, stabilities and magnetic properties of iron oxide clusters (FeO) n μ (n = 1–8, μ = 0, ±1): insights and perspectives. *RSC Adv.* 5, 6560–6570. doi: 10.1039/C4RA12259C

Kitsopoulos, A., Chick, C. J., Zhao, Y., and Neumark, D. M. (1991). Study of the low-lying electronic states of Si_2 and Si_2^- using negative ion photodetachment techniques. *J. Chem. Phys.* 95, 1441–1448. doi: 10.1063/1.461057

Lu, C., and Chen, C. (2018). High-pressure evolution of crystal bonding structures and properties of feooh. *J. Phys. Chem. Lett.* 9, 2181–2185. doi: 10.1021/acs.jpclett.8b00947

Lu, C., Li, Q., Ma, Y., and Chen, C. (2017). Extraordinary indentation strain stiffening produces superhard tungsten nitrides. *Phys. Rev. Lett.* 119:115503. doi: 10.1103/PhysRevLett.119.115503

Lu, C., Maximilian, A., and Changfeng, C. (2018). Unraveling the structure and bonding evolution of the newly discovered iron oxide FeO_2. *Phys. Rev. B* 98:054102. doi: 10.1103/PhysRevB.98.054102

Lu, C., Miao, M., and Ma, Y. (2013). Structural evolution of carbon dioxide under high pressure. *J. Am. Chem. Soc.* 135, 14167–14171. doi: 10.1021/ja404854x

Lv, J., Wang, Y., Zhu, L., and Ma, Y. (2012). Particle-swarm structure prediction on clusters. *J. Chem. Phys.* 137:084104. doi: 10.1063/1.4746757

Morris, R. G., Redin, R. D., and Danielson, G. C. (1958). Semiconducting properties of Mg_2Si single crystals. *Phys. Rev. B* 109:1916. doi: 10.1103/PhysRev.109.1909

Pearson, R. G. (1997). *Chemical Hardness - Applications From Molecules to Solids*. Weinheim: Wiley-VCH, 198.

Ruette, F., Sánchez, M., Anez, R., Bermúdez, A., and Sierraalta, A. (2005). Diatomic molecule data for parametric methods. I. *J. Mol. Struct. THEOCHEM* 729, 19–37. doi: 10.1016/j.theochem.2005.04.024

Song, S. W., Striebel, K., and Cairns, E. (2003). Electrochemical studies of the Mg_2Si thin films prepared with pulsed laser deposition. *J. Electrochem. Soc.* 153, A12–A19. doi: 10.1149/1.1527937

Sun, W., Xia, X., Lu, C., Kuang, X., and Hermann, A. (2018). Probing the structural and electronic properties of zirconium doped boron clusters: Zr distorted B 12 ligand framework. *Phys. Chem. Chem. Phys.* 20, 23740–23746. doi: 10.1039/C8CP03384F

Sun, W. G., Wang, J. J., Lu, C., Xia, X. X., Kuang, X. Y., and Hermann, A. (2017). Evolution of the structural and electronic properties of medium-sized sodium clusters: a honeycomb-like na\r, 20\r, cluster. *Inorg. Chem.* 56, 1241–1248. doi: 10.1021/acs.inorgchem.6b02340

Trivedi, R., Dhaka, K., and Bandyopadhyay, D. (2014). Study of electronic properties, stabilities and magnetic quenching of molybdenum-doped germanium clusters: a density functional investigation. *RSC Adv.* 4, 64825–64834. doi: 10.1039/C4RA11825A

Wang, Y., Lv, J., Zhu, L., and Ma, Y. (2010). Crystal structure prediction via particle-swarm optimization. *Phys. Rev. B* 82:094116. doi: 10.1103/PhysRevB.82.094116

Wang, Y., Lv, J., Zhu, L., and Ma, Y. (2012). CALYPSO: a method for crystal structure prediction. *Comput. Phys. Commun.* 183, 2063–2070. doi: 10.1016/j.cpc.2012.05.008

Wittmer, M., Lüthy, W., and Allmen, M. V. (1979). Laser induced reaction of magnesium with silicon. *Phys. Lett. A* 75, 127–130. doi: 10.1016/0375-9601(79)90300-1

Xia, X. X., Hermann, A., Kuang, X. Y., Jin, Y. Y., Lu, C., and Xing, X. D. (2015). Study of the structural and electronic properties of neutral and charged niobium-doped silicon clusters: niobium encapsulated in silicon cages. *J. Phys. Chem. C* 120, 677–684. doi: 10.1021/acs.jpcc.5b09453

Xiao, T., Weiguo, S., Yuantong, G., Lu, C., Liangzhi, K., and Changfeng, C. (2019). CoB_6 monolayer: a robust two-dimensional ferromagnet. *Phys. Rev. B* 99:045445. doi: 10.1103/PhysRevB.99.045445

Xing, X., Hermann, A., Kuang, X., Ju, M., Lu, C., Jin, Y., et al. (2016a). Insights into the geometries, electronic and magnetic properties of neutral and charged palladium clusters. *Sci. Rep.* 6:19656. doi: 10.1038/srep19656

Xing, X., Wang, J., Kuang, X., Xia, X., Lu, C., and Maroulis, G. (2016b). Probing the low-energy structures of aluminum–magnesium alloy clusters: a detailed study. *Phys. Chem. Chem. Phys.* 18, 26177–26183. doi: 10.1039/C6CP05571K

Yang, J., Li, B., and Zhan, S. (2006). Study of gaas cluster ions using fp-lmto md method. *Phys. Lett. A* 348, 416–423. doi: 10.1016/j.physleta.2005.08.071

Zhang, S., Zhang, Y., Yang, X., Lu, C., Li, G., and Lu, Z. (2015). Systematic theoretical investigation of structures, stabilities, and electronic properties of rhodium-doped silicon clusters: Rh 2 Si n q (n = 1–10; q = 0, ±1). *J. Mater. Sci.* 50, 6180–6196. doi: 10.1007/s10853-015-9175-x